processes

MDPI

Article

A Study on Flow Field Characteristics and Air Purifier with Barrier Effects

Yu-Ling Liu [1], Yean-Der Kuan [2,*] and Win-Jet Luo [3]

[1] Ph.D. Program, Intelligent Machinery and Smart Manufacturing, National Chin-Yi University of Technology, Taichung City 41170, Taiwan; sla8t1003@student.ncut.edu.tw
[2] Department of Refrigeration, Air Conditioning and Energy Engineering, National Chin-Yi University of Technology, Taichung City 41170, Taiwan
[3] Graduate Institute of Precision Manufacturing, National Chin-Yi University of Technology, Taichung City 41170, Taiwan; wjluo@ncut.edu.tw
* Correspondence: ydkuan@ncut.edu.tw; Tel.: +886-4-23924505 (ext. 8256)

Abstract: An air curtain machine is used in the entrances and exits of public places where air conditioners are used. The high-speed centrifugal or axial fan blows out the air, creating an airflow barrier to prevent air convection inside and outside, reducing air conditioning losses, and maintaining the indoor air quality by preventing dust, insects, and harmful gases from entering the room. Observation of the airflow behavior was conducted using CFD simulation, to explore whether it has a blocking effect, and the air curtain principle was applied to the air purification equipment. It is mainly composed of several rows of arrayed hole air outlets to form a multi-composite air wall. The airflow on the two sides, or below, can be blocked by the composite air wall and integrated into the main airflow, so that the air walls will not affect each other, and form a barrier effect to prevent infection. This research includes the measurement of impedance characteristics for three layers of filters made of different materials. These filters are used as the input characteristic parameters in the simulation analysis. Four scenarios are discussed, including the consultation room, hospital ward, quarantine station, and conference room. From the simulation results, it is known that when there are many people, the equipment can be set to high speed to increase the volume of air, forming a wind wall to effectively block airflow from the people in the chairs, reducing the risk of infection. Note that the rotation speed should not be too high. The air outlet equipment is susceptible to turbulent flow, which will make the airflow deviate from the expected direction and increase the possibility of mutual infection between adjacent people. Partitions can be used to block airflow to reduce the risk of infection.

Keywords: air purifier; computational fluid dynamics; air quality; flow behavior; simulation analysis

Citation: Liu, Y.-L.; Kuan, Y.-D.; Luo, W.-J. A Study on Flow Field Characteristics and Air Purifier with Barrier Effects. *Processes* **2022**, *10*, 864. https://doi.org/10.3390/pr10050864

Academic Editor: Farhad Ein-Mozaffari

Received: 10 March 2022
Accepted: 21 April 2022
Published: 27 April 2022

1. Introduction

Air quality issues have received considerable attention in Taiwan in recent years. Under the influence of global warming and the greenhouse effect, the outdoor temperature has become relatively high. People now prefer to stay indoors for activities. Natural ventilation or air conditioners can be utilized for indoor ventilation to make the human body feel relatively comfortable. However, in indoor spaces, doors and windows must be closed when air conditioners are used. This produces confined spaces, resulting in problems such as air quality deterioration and physical discomfort. Air filtration to maintain good indoor air quality is the subject explored in this study [1–8].

In March 2020, COVID-19 (coronavirus disease 2019) began ravaging the world and has rapidly developed ever since, attracting significant attention from all countries worldwide. The main COVID-19 infection transmission method is through viral droplets expelled during human-to-human contact. Nosocomial infection cases are of great concern to the general public, increasing the suspicion that hospitals are places with a high risk of infection.

Hence, the air curtain principle is applied to simulate an air purifier flow field analysis with barrier effects, using computational fluid dynamics (CFD) to conduct flow field analyses in various scenarios, such as consulting rooms, hospital wards, quarantine stations, and conference rooms. The air purifier is used to filter harmful substances from the indoor air. After filtering, airflow with a certain velocity is blown out from the air purifier outlet fan to form an air wall. An air wall can also be formed by blocking or changing the flow direction, which can reduce the chance of air droplet infection. This study analyzed airflow fields and investigated whether an air purifier can effectively filter viruses under various simulation scenarios [9–21].

Most people think that the effect of ambient air purification depends on the equipment's filtering system, ignoring the overall air circulation effect on the environment. After the air is expelled from, and then returned to, the air purifier, a virus can spread among a crowd. The air purification device forms a barrier curtain, which drives the airflow in the same direction, to prevent droplets from interacting with the air inhaled by the human body. This paper discusses an air purifier design based on the air curtain principle. This air purifier can be used in small, confined spaces, such as consulting rooms and hospital wards, as well as open spaces where large numbers of people gather, such as quarantine spaces. Vaccine administration stations and CFD simulations were used to observe the flow fields of entire spaces, to explore whether a blocking effect exists, as an important reference for future applications.

2. Research Method

This paper simulated an air purifier with barrier effects and compared the experimental results using a numerical simulation analysis. This study carried out wind tunnel experiments for different filter screens and air purifier fans. Static pressure–flow curves (P-Q curves) were formed by measuring all the points, and the measured P-Q curve values were used to set the simulation parameters for comparison and discussion, as shown in Figure 1.

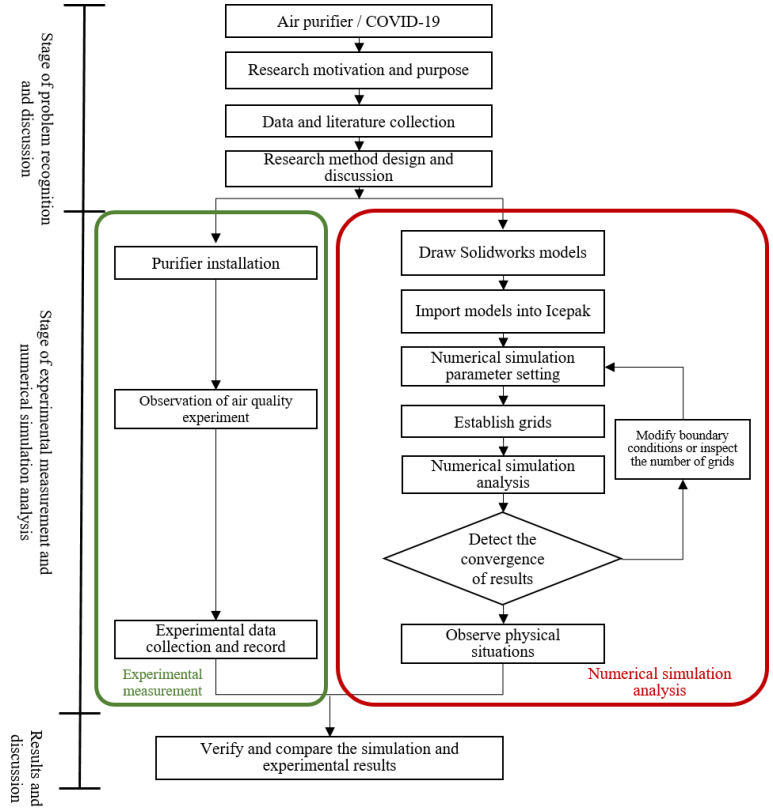

Figure 1. Air purifier research process and architecture.

2.1. CFD Simulation Analysis

After modeling with SOLIDWORKS (Dassault Systèmes SOLIDWORKS Corp. Waltham, MA, USA), the files were imported into ANSYS ICEPAK (ANSYS, Inc., Canonsburg, PA, USA) to establish the flow field simulation scenario space. Computational fluid dynamics (CFD) uses a computer to establish grid points and provide appropriate simulated fluids, including the velocity, concentration, pressure, etc. The main governing equations between the flow fields are the continuous, momentum, kinetic energy transfer, and dissipation equations, such as Equations (1)–(8) [22].

Continuous equation:

$$\frac{\partial \mu}{\partial x} + \frac{\partial v}{\partial y} + \frac{\partial w}{\partial z} = 0 \tag{1}$$

Momentum equation:

$$x : \rho\left(\mu\frac{\partial u}{\partial x} + v\frac{\partial u}{\partial y} + w\frac{\partial u}{\partial z}\right) = -\frac{\partial p}{\partial x} + u\left(\frac{\partial^2 u}{\partial x^2} + \frac{\partial^2 u}{\partial y^2} + \frac{\partial^2 u}{\partial z^2}\right) \tag{2}$$

$$y : \rho\left(\mu\frac{\partial v}{\partial x} + v\frac{\partial v}{\partial y} + w\frac{\partial v}{\partial z}\right) = -\frac{\partial p}{\partial y} + pg + u\left(\frac{\partial^2 v}{\partial x^2} + \frac{\partial^2 v}{\partial y^2} + \frac{\partial^2 v}{\partial z^2}\right) \tag{3}$$

$$z : \rho\left(\mu\frac{\partial w}{\partial x} + v\frac{\partial w}{\partial y} + w\frac{\partial w}{\partial z}\right) = -\frac{\partial p}{\partial z} + u\left(\frac{\partial^2 w}{\partial x^2} + \frac{\partial^2 w}{\partial y^2} + \frac{\partial^2 w}{\partial z^2}\right) \tag{4}$$

Turbulent kinetic energy transfer equation and dissipation equation:

$$\rho\left(\mu\frac{\partial k}{\partial x} + v\frac{\partial k}{\partial y}w\frac{\partial k}{\partial z}\right) = \left(\mu + \frac{\mu_t}{\sigma_k}\right)\left(\frac{\partial^2 k}{\partial x^2} + \frac{\partial^2 k}{\partial y^2} + \frac{\partial^2 k}{\partial z^2}\right) + G_k - \widetilde{\varepsilon} \tag{5}$$

$$\rho\left(\mu\frac{\partial \varepsilon}{\partial x} + v\frac{\partial \varepsilon}{\partial y}w\frac{\partial \varepsilon}{\partial z}\right) = \left(\mu + \frac{\mu_t}{\sigma_\varepsilon}\right)\left(\frac{\partial^2 \varepsilon}{\partial x^2} + \frac{\partial^2 \varepsilon}{\partial y^2} + \frac{\partial^2 \varepsilon}{\partial z^2}\right) + C_1\frac{\varepsilon}{k}G_k - C_2\frac{\varepsilon^2}{k} \tag{6}$$

$$G_k = \rho\left(\mu'^2\frac{\partial u}{\partial x} + u'v'^{\frac{\partial v}{\partial x}} + u'w'^{\frac{\partial w}{\partial x}} + u'v'^{\frac{\partial u}{\partial y}} + v'^2\frac{\partial v}{\partial y} + v'w'^{\frac{\partial w}{\partial y}} + u'w'^{\frac{\partial u}{\partial z}} + u'w'^{\frac{\partial v}{\partial z}} + w'^2\frac{\partial w}{\partial z}\right) \tag{7}$$

$$\widetilde{\varepsilon} = \mu\left\{2\left[\left(\frac{\partial u'}{\partial x}\right)^2 + \left(\frac{\partial v'}{\partial y}\right)^2 + \left(\frac{\partial w'}{\partial z}\right)^2\right] + \left(\frac{\partial u'}{\partial y} + \frac{\partial v'}{\partial x}\right)^2 + \left(\frac{\partial u'}{\partial y} + \frac{\partial v'}{\partial x}\right)^2 + \left(\frac{\partial v'}{\partial z} + \frac{\partial w'}{\partial y}\right)^2\right\} \tag{8}$$

The boundary conditions (location) for this space are 3.0 m in length, 4.3 m in width, and 2.0 m in height. The spatial concentration (species definitions) and water concentration (H_2O) are both set to 0.04. The human body's exhalation port (opening) is a circle with a diameter of 0.1 m. The body's exhalation port velocity (flow specification) is set to 10.0 m/s. The above are all fixed conditions. This study uses the mixture to set the simulation parameters, which are the continuity equation, the momentum equation, and the quadratic image volume equation, such as Equations (9)–(15) [22].

Continuity equation:

$$\frac{\partial}{\partial_t}(\rho m) + \nabla \cdot (\rho_m \vec{v}_m) = 0 \tag{9}$$

where $\vec{v}_m$ is the mass-averaged velocity:

$$\vec{v}_m = \frac{\sum_{k=1}^{n} \alpha_k \rho_k \vec{v}_k}{\rho_m} \tag{10}$$

ρ_m is the mixture density:

$$\rho_m = \sum_{k=1}^{n} \alpha_k \rho_k \tag{11}$$

α_k is the volume fraction of phase k.

Momentum equation:

$$\frac{\partial}{\partial t}\left(\rho_m \vec{v}_m\right) + \nabla\cdot\left(\rho_m \vec{v}_m \vec{v}_m\right) = -\nabla p + \nabla\cdot\left[\left(\nabla \vec{v}_m + \nabla \vec{v}_m^{\,T}\right)\right] + \rho_m \vec{g} + \vec{F} + \nabla\cdot\left(\sum_{k=1}^{n} \alpha_k \rho_k \vec{v}_{dr,k} \vec{v}_{dr,k}\right) \quad (12)$$

where n is the number of phases, $\vec{F}$ is the body force, and μ_m is the mixture viscosity:

$$\mu_m = \sum_{k=1}^{n} \alpha_k \mu_k \quad (13)$$

$\vec{v}_{dr,k}$ is the drift velocity for secondary phase k:

$$\vec{v}_{dr,k} = \vec{v}_k - \vec{v}_k \quad (14)$$

Volume fraction equation for the secondary phases:

$$\frac{\partial}{\partial t}\left(\alpha_p \rho_p\right) + \nabla\cdot\left(\alpha_p \rho_p \vec{v}_{dr,p}\right) + \sum_{q=1}^{n}\left(\dot{m}_{qp} - \dot{m}_{pq}\right) \quad (15)$$

Figure 2 is an air purification equipment model diagram. The air outlet size in the figure is set to 0.8 m long and 0.59 m wide. The equipment contains filters made of different materials. Figure 3 shows that the filters are divided into A, B, and C, with three different filter materials. The model's size is 0.77 m long and 0.61 m wide. The model's thickness is 0.02 m, 0.075 m, and 0.015 m thick, respectively.

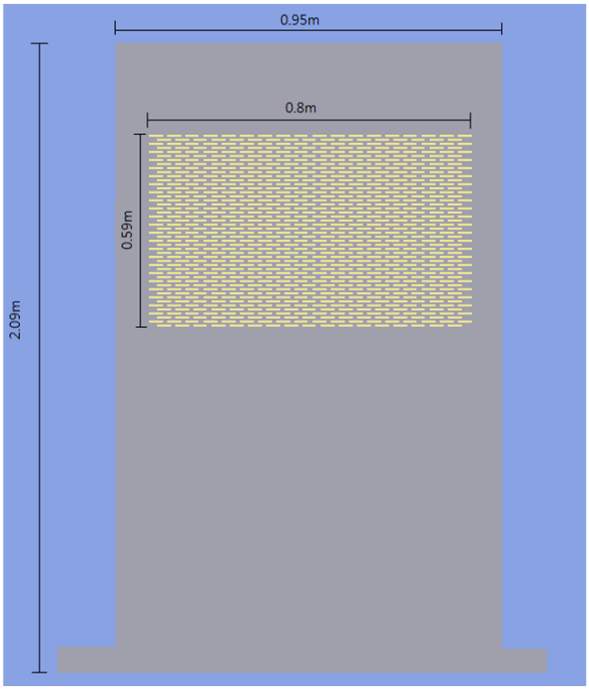

Figure 2. Air purifier model diagram (front).

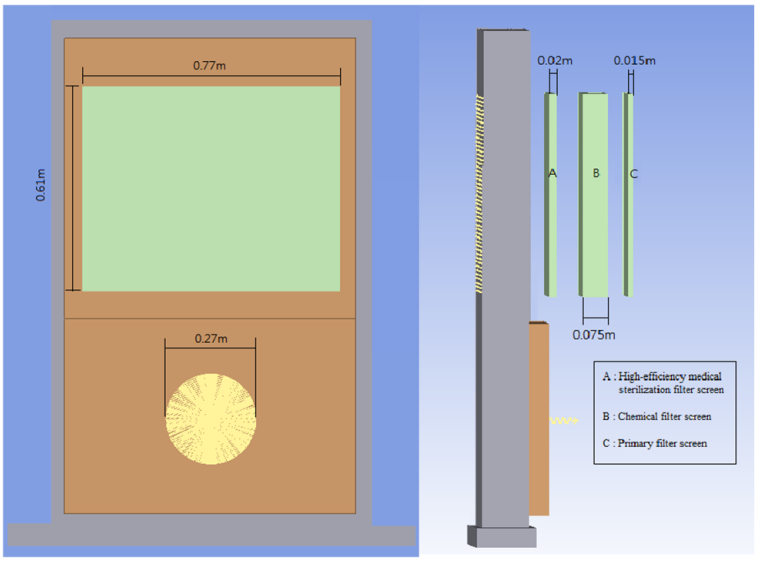

Figure 3. Air purifier filter setting diagram.

The flow field simulation has four main scenarios (Case 1~Case 4): consulting rooms, hospital wards, quarantine stations, and conference rooms. The size of the four situational spaces is based on the school's medical room as a boundary reference setting sample.

Figure 4 is a schematic diagram of the consultation room (Case 1). The distance between the human body's exhalation port and the floor is from point A to point C, with a 1.0 m set value. The interpersonal distance is 1.4 m from point A to point B, with the exhalation port as the center. The human body's exhalation port airflow direction at point A is from point A to point B. The human body's exhalation port airflow direction at point B is from point B to point A. The air purifier airflow outlet is shown at point D. The air inlet position is as shown at point E. This is a closed space.

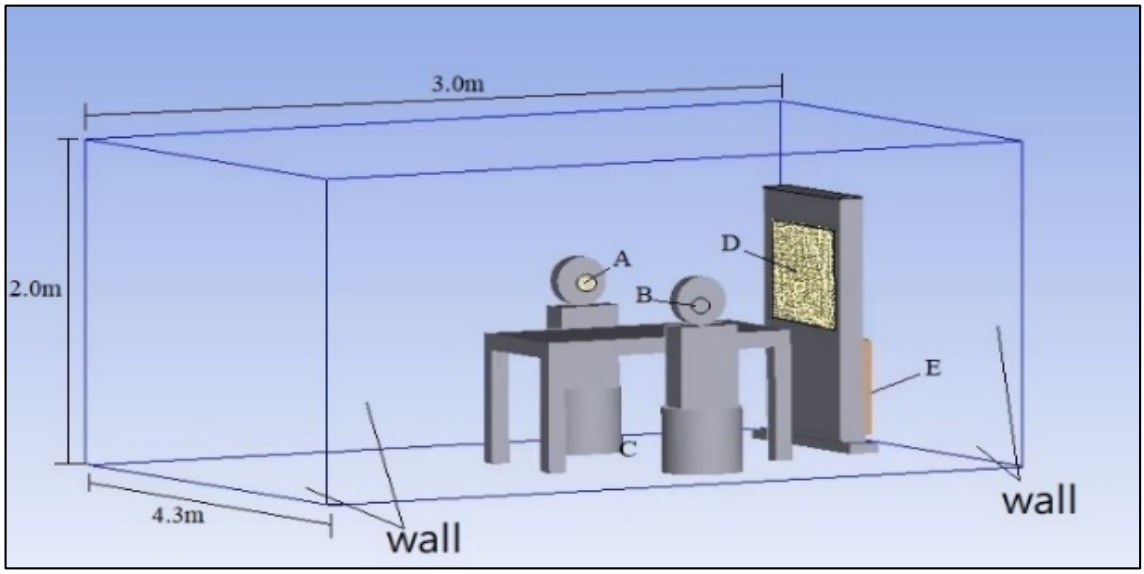

Figure 4. Air purifier in the consulting room.

Figure 5 is a schematic diagram of the hospital ward (Case 2). The distance between the human body's exhalation port and the floor is from point A to point C, with a 1.33 m set value. The distance between the human body's exhalation port and the floor is from point B to point D, with a 0.92 m set value. At point A, the airflow direction is from the human body's exhalation port in the direction of the arrow in the figure. At point B, the airflow

direction from the human body's exhalation port is vertically upward. The interpersonal distance is set to 0.7 m from point A to point B, with the exhalation as the center. The air purifier airflow outlet position is shown at point E. The air inlet position is shown at point F. This space is closed.

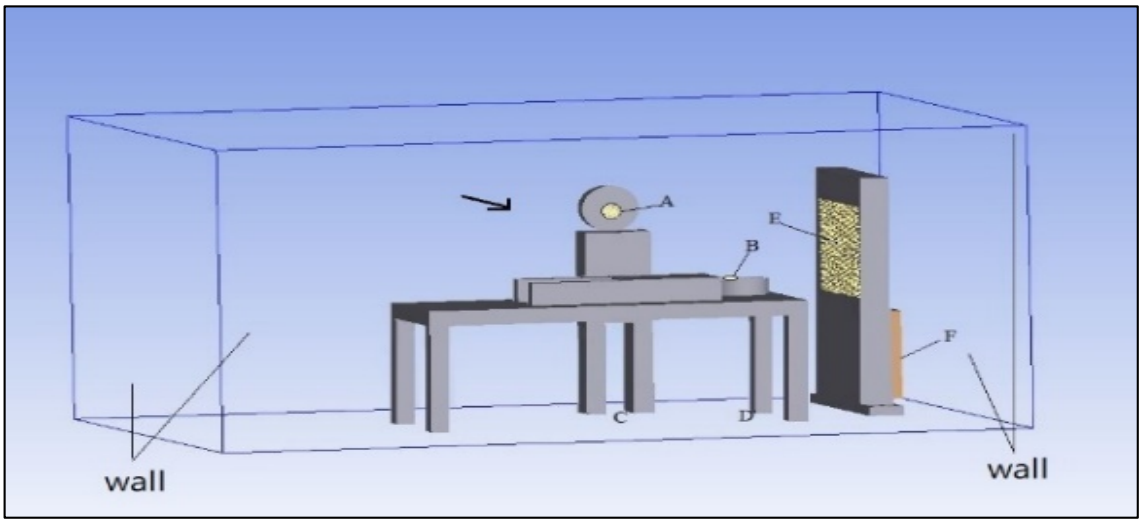

Figure 5. Air purifier in the ward.

Figure 6 is a schematic diagram of the quarantine station (Case 3). The distance between the human body's exhalation port and the floor is from point A to point C, with a 1.0 m set value. The interpersonal distance is 1.4 m from point A to point B, with the exhalation port as the center. The airflow direction from the human body's exhalation port at point A is from point A to point B. The human body's exhalation port airflow direction at point B is from point B to point A. The air purifier airflow outlet is shown at point D. The air inlet position is as shown at point E. This space is semi-open. The F and G surfaces are set as ventilation grilles for the ventilation space.

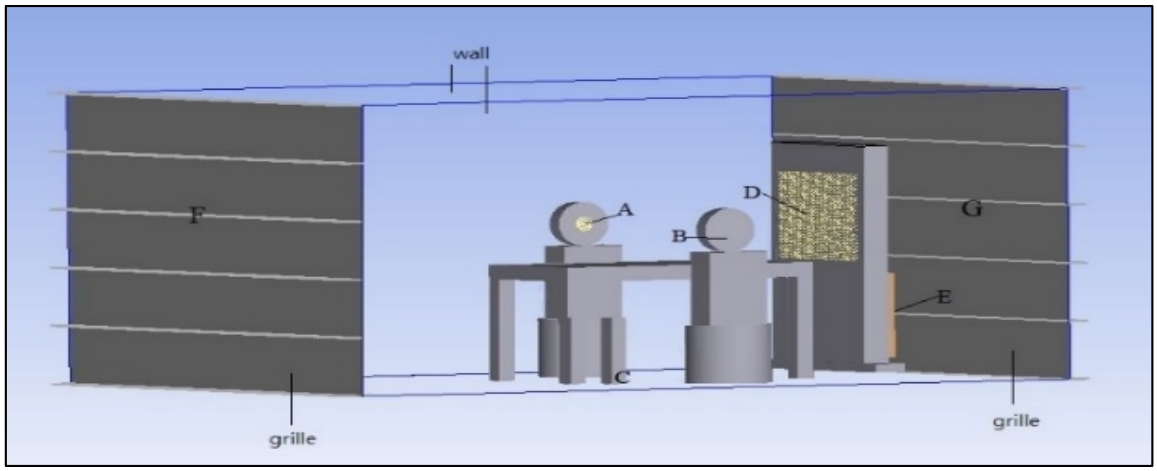

Figure 6. Air purifier in the quarantine station.

Figure 7 is a schematic diagram of the conference room (Case 4). The distance between the human body's exhalation port and the floor is from point A to point G, with a 1.0 m set value (the other five settings are the same). The distance between people sitting at the table is 1.4 m from point A to point B, with the exhalation port as the center. The airflow direction from the human body's exhalation port at point A is from point A to point B. The airflow direction from the human body's exhalation port at point B is from point B to point

A. The remaining two groups are the same. The interpersonal distance is 1.0 m from point A to point C, with the exhalation port as the center (the other five settings are the same). The air purifier airflow outlet is shown at point H. The air inlet position is as shown at point I, and this is a closed space.

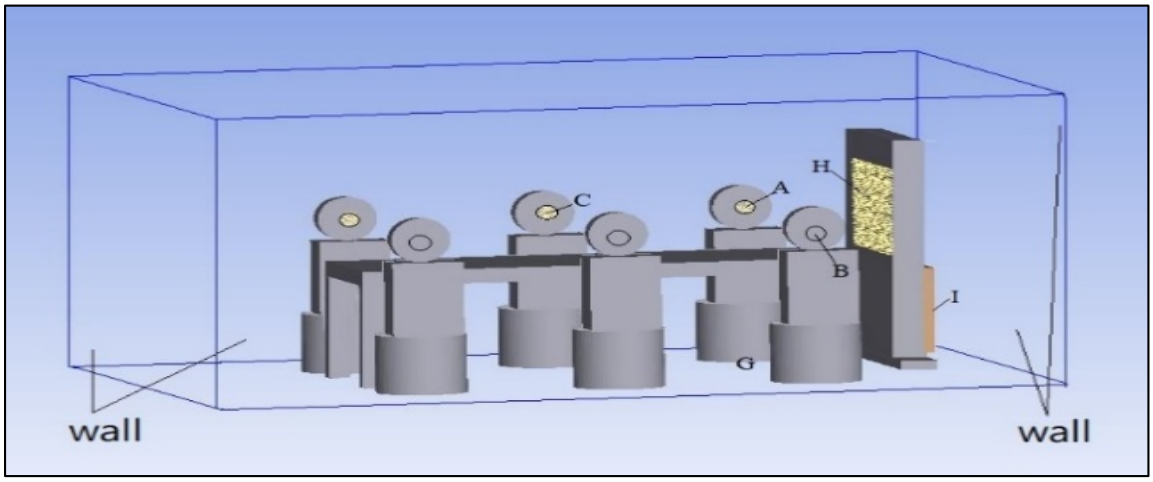

Figure 7. Air purifier in the conference room.

The fan pressure and air volume at various speeds were measured experimentally through a wind tunnel, as shown in Figure 8. Tables can be produced using the wind tunnel experiments, as shown in Table 1. The air volume and pressure values at each rotation speed were obtained. The *X*-axis and *Y*-axis were drawn as the air volume (CMM) and the P-Q curve of pressure (Pa), respectively, as shown in Figures 9–11. ANSYS ICEPAK was employed for the simulation analysis. The steady-state flow field results were analyzed using the changes in pressure and velocity caused by convection [23].

Figure 8. Wind tunnel experiment setup diagram of fan.

Table 1. Pressure and air volume of the air purifier at different rotation speeds.

	Measuring Points	1	2	3	4	5	6	7	8	9
Low rotation speed (LOW)	Air volume (CMM)	0	0.5960	1.0621	1.6743	2.2525	2.7259	2.7810	2.8361	2.8912
	Pressure (in water)	0.4770	0.4025	0.3759	0.3158	0.2821	0.2484	0.2464	0.2447	0.2435
Medium rotation speed (MEDIUM)	Air volume (CMM)	0	0.8493	1.5122	2.3666	3.2118	3.5712	3.6388	3.7063	3.7747
	Pressure (in water)	0.7647	0.7163	0.6036	0.5292	0.4640	0.4453	0.4404	0.4354	0.4308
High rotation speed (HIGH)	Air volume (CMM)	0	1.3381	2.5906	3.5166	5.1802	6.0373	6.2046	6.3703	6.5371
	Pressure (in water)	1.1774	1.0498	1.0105	0.9395	0.8245	0.7629	0.7510	0.7386	0.7271

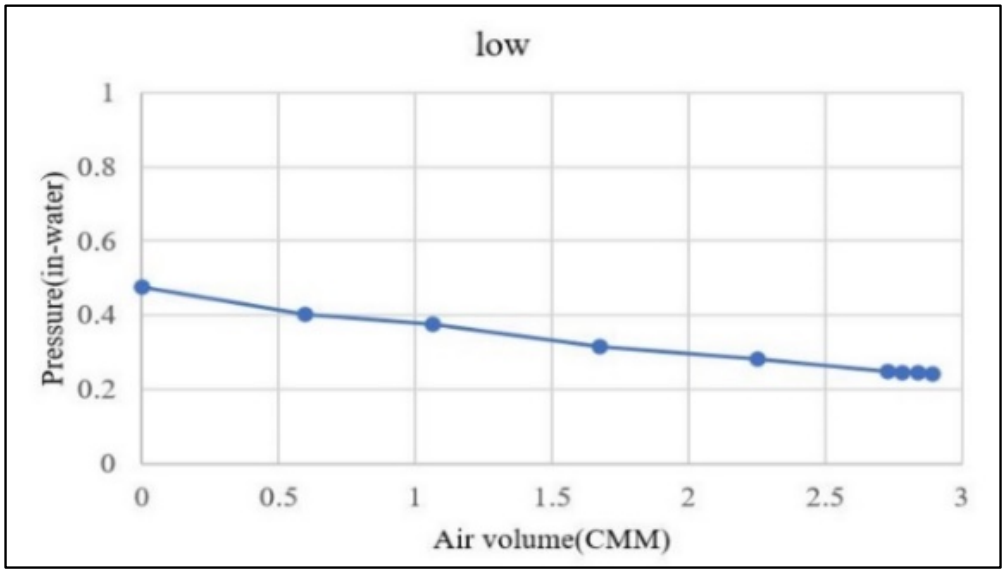

Figure 9. P-Q curve of the air purifier at a low rotation speed.

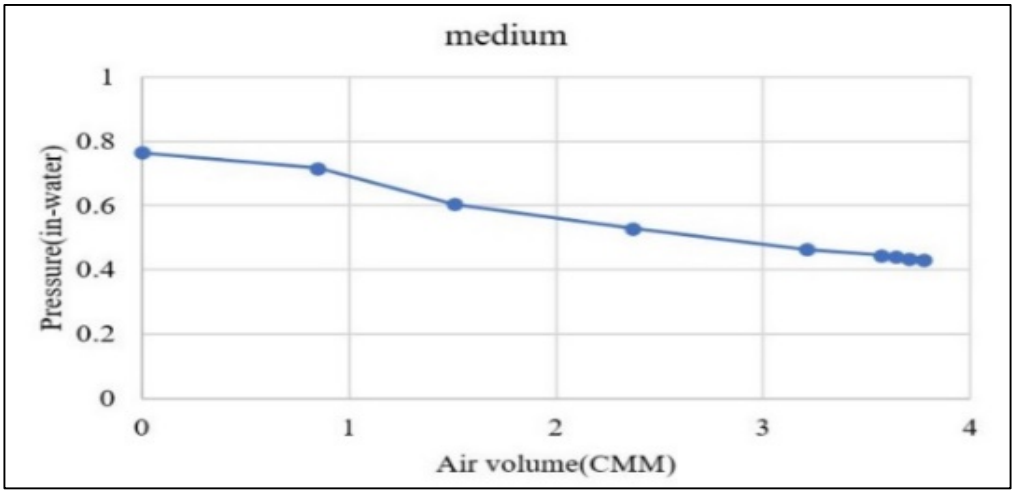

Figure 10. P-Q curve of the air purifier at a medium rotation speed.

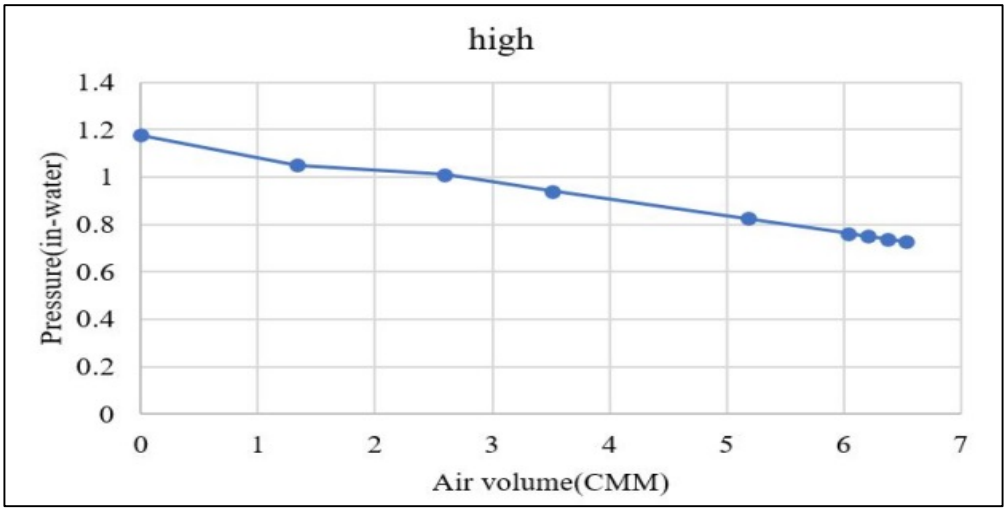

Figure 11. P-Q curve of the air purifier at a high rotation speed.

2.2. Impedance Characteristics of Filter Screens Measured with Different Materials

In order to confirm the validity of the flow field simulation input parameters, an air purifier filter screen performance test was carried out using the wind tunnel experiment, as shown in Figure 12. Three different filter screen materials were installed in the equipment. The equipment had filter screens constructed of three layers using different materials, including a primary filter screen, chemical filter screen, and high-efficiency medical sterilization filter screen, as shown in Figures 13–15. The performances of the different filter screen materials were measured, as shown in Table 2. The filter screens' velocity and pressure for all materials were obtained, while the *X*-axis and *Y*-axis were drawn as the velocity (m/s) and the P-Q curve of pressure (Pa), respectively, as shown in Figures 16–18. Other technical principles were used for the filter screens of different materials, with the descriptions shown in Table 3 [24].

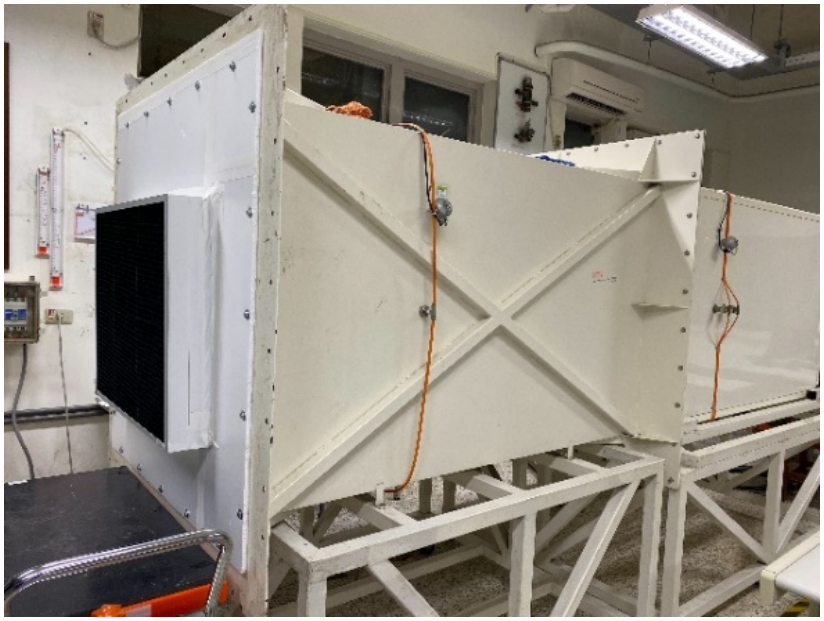

Figure 12. Experiment filter wind tunnel setup.

Figure 13. High-efficiency medical sterilization filter screen.

Figure 14. Chemical filter screen.

Figure 15. Primary filter screen.

Table 2. Air purifier filter screen pressure and air volume.

	Measuring Points	**1**	**2**	**3**	**4**	**5**	**6**	**7**	**8**	**9**
High-efficiency medical sterilization filter screen (inner)	Velocity (m/s)	0	0.0145	0.0259	-	-	-	-	-	-
	Pressure (in water)	0	0.001	0.003	-	-	-	-	-	-
Chemical filter screen (middle)	Velocity (m/s)	0	0.0145	0.021	0.0323	0.0407	0.047	0.0478	0.0487	0.0495
	Pressure (in water)	0	0.001	0.002	0.005	0.008	0.010	0.011	0.011	0.012
Primary filter screen (outer)	Velocity (m/s))	0	0.0064	0.0145	0.0209	0.0258	0.0323	0.0331	0.0339	0.0347
	Pressure (in water)	0	0.002	0.010	0.021	0.032	0.049	0.052	0.054	0.057

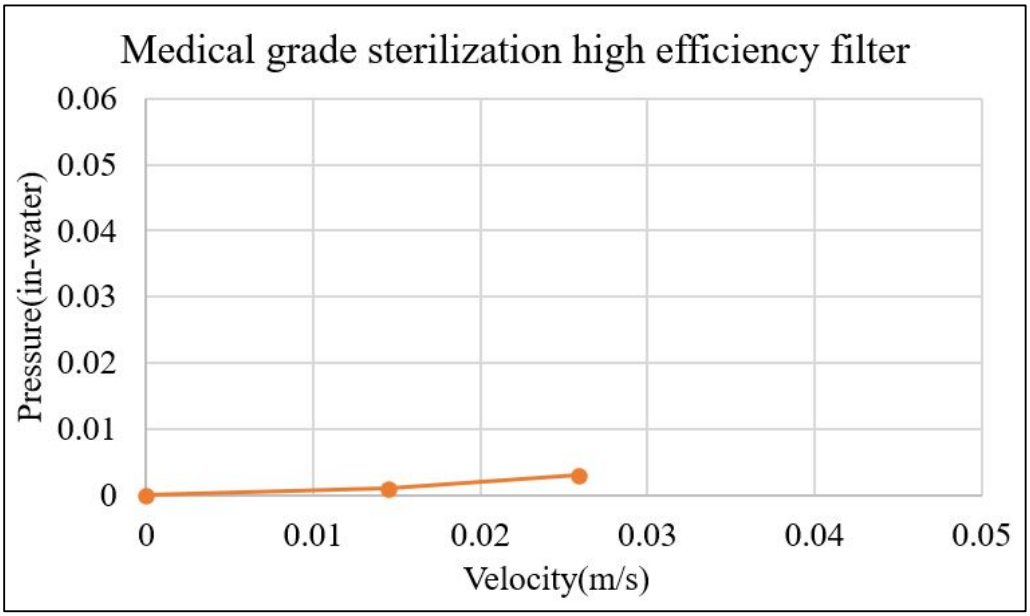

Figure 16. P-Q curve of the high-efficiency medical sterilization filter screen.

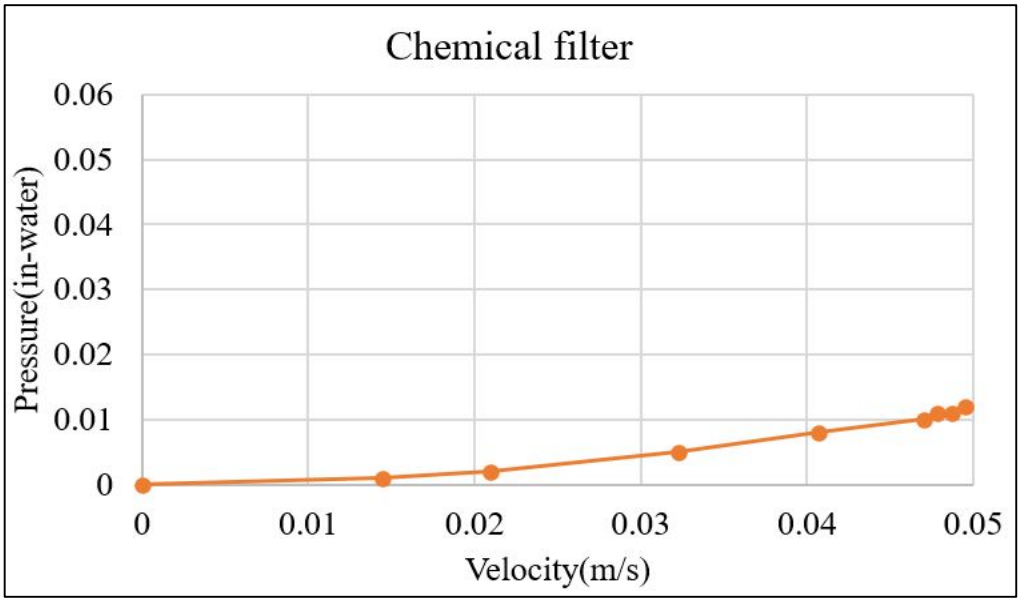

Figure 17. P-Q curve of the chemical filter screen.

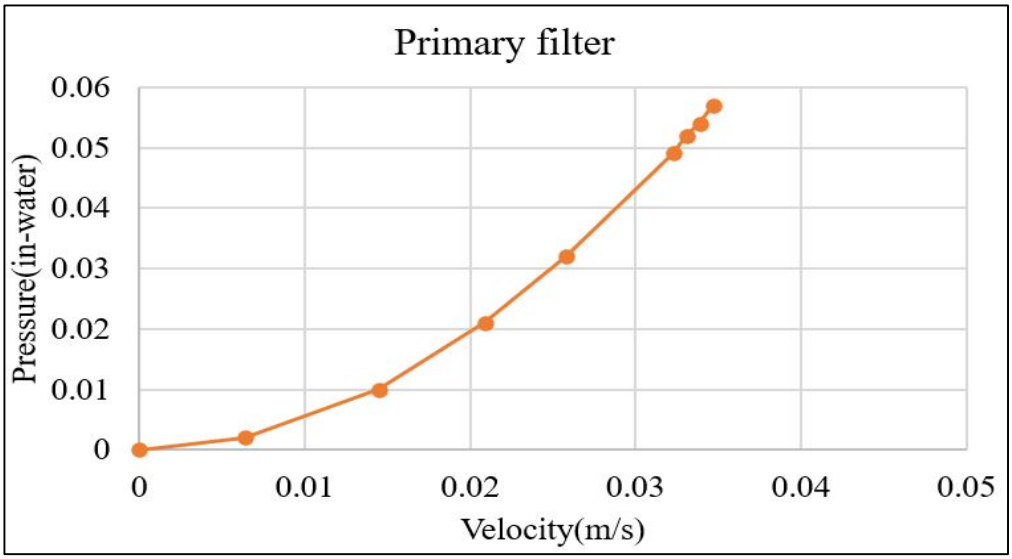

Figure 18. P-Q curve of the primary filter screen.

Table 3. Technical principles for air purifier filter screens [24].

Filter Screen Name	High-Efficiency Medical Sterilization Filter Screen	Chemical Filter Screen	Primary Filter Screen
Technical principles	The high-efficiency silver ion cleaning system filters $PM_{2.5}$ and $PM_{0.3}$, to achieve the sterilization effect effectively.	Filter formaldehyde and ozone, and effectively adsorb harmful substances, such as formaldehyde and ozone, to completely remove odor and maintain a fresh and clean medical environment.	Filter large particles, such as dust and floating objects in the air, to improve the service life of other filters.

3. Results and Discussion

This study simulated four different human environment scenarios, including consulting rooms, hospital wards, quarantine stations, and conference rooms. The details for each scenario are described as follows:

Case 1: The air purifier was set to run at a low rotation speed. The gases emitted by the human body in a confined space flowed back to the suction end of the equipment, along with the airflow direction, to produce a circulation effect. As shown in Figure 19, a simulation top view, the indoor air could enter the equipment for circulation and filtration.

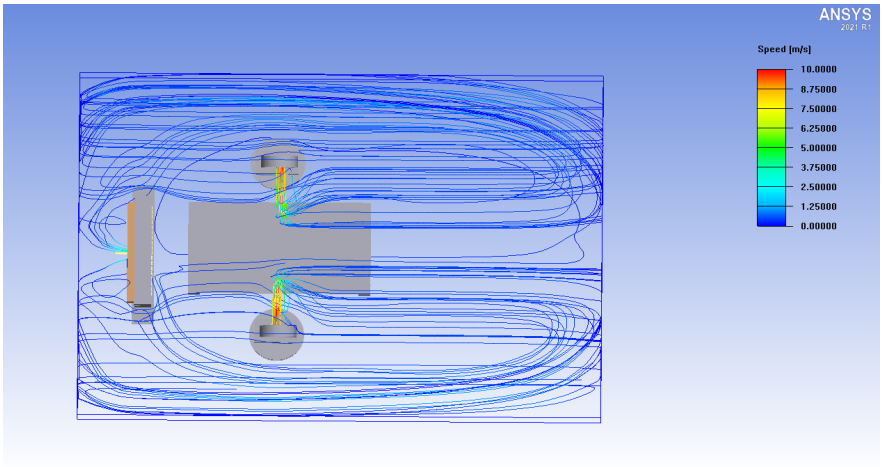

Figure 19. Air purifier simulation top view in the consulting room at a low rotation speed.

In the same scenario, at a high rotation speed, the airflow from the equipment air outlet is enhanced to form a gas wall, which effectively blocks and blows away the gas exhaled by the human body, as shown in Figures 20 and 21. Due to the high pressure, the gas exhaled by the human body is brought into the filter suction end and the airflow for circulating filtration.

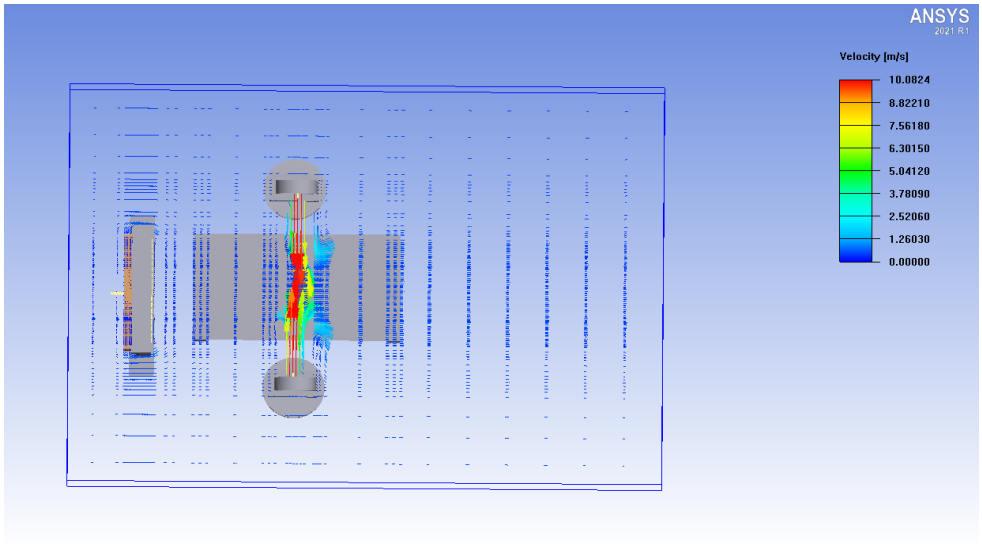

Figure 20. Air purifier top-view simulation in the consulting room at a high rotation speed −1.

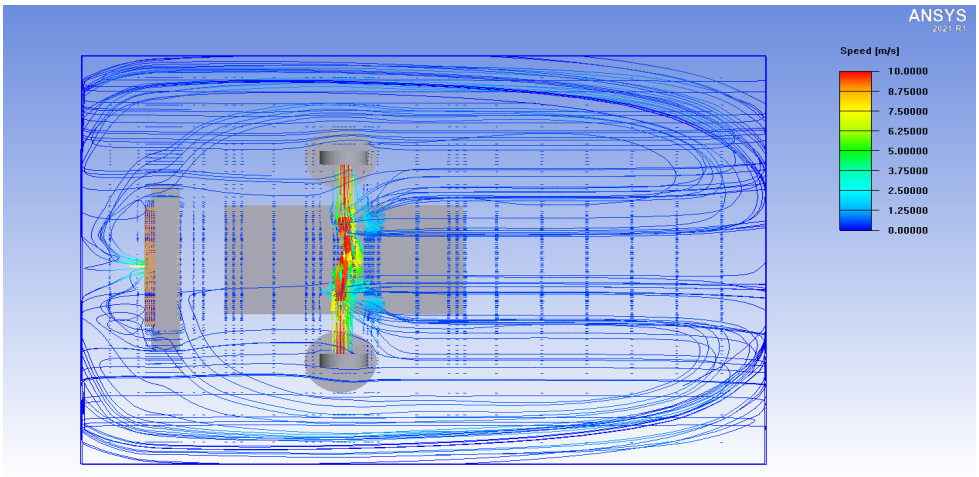

Figure 21. Air purifier top-view simulation in the consulting room at a high rotation speed −2.

Case 2: An air purifier was installed in the hospital ward. It was designed for patients lying on a sickbed with doctors making bedside diagnoses, and the purifier was set at a low rotation speed for air purification. From the outlet velocity, the air discharged by the equipment could carry away the gases emitted by the human body, as shown in Figure 22 in the top-view simulation. The gases emitted by the human body in a confined space had circulation effects, so that the indoor air could enter the equipment for filtration and then be discharged, as shown in Figure 23.

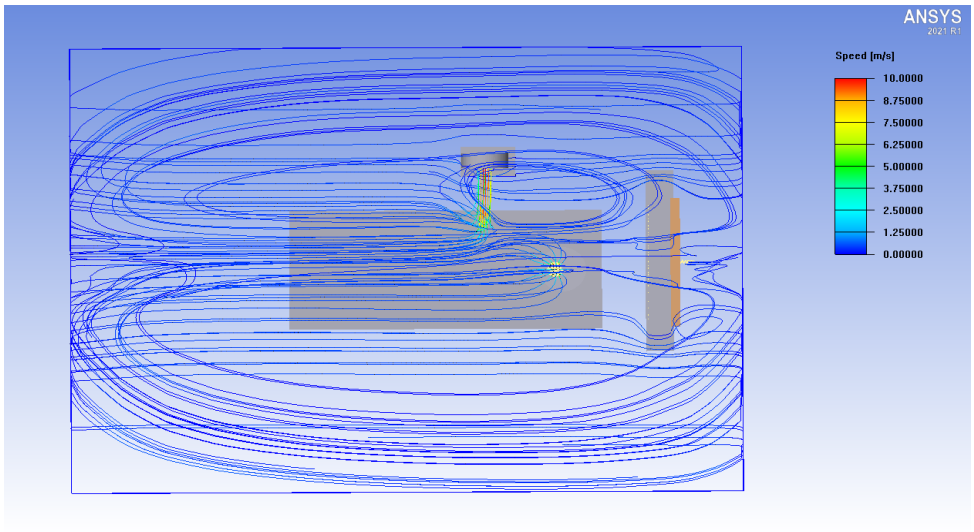

Figure 22. Air purifier top-view simulation in the ward at a low rotation speed −1.

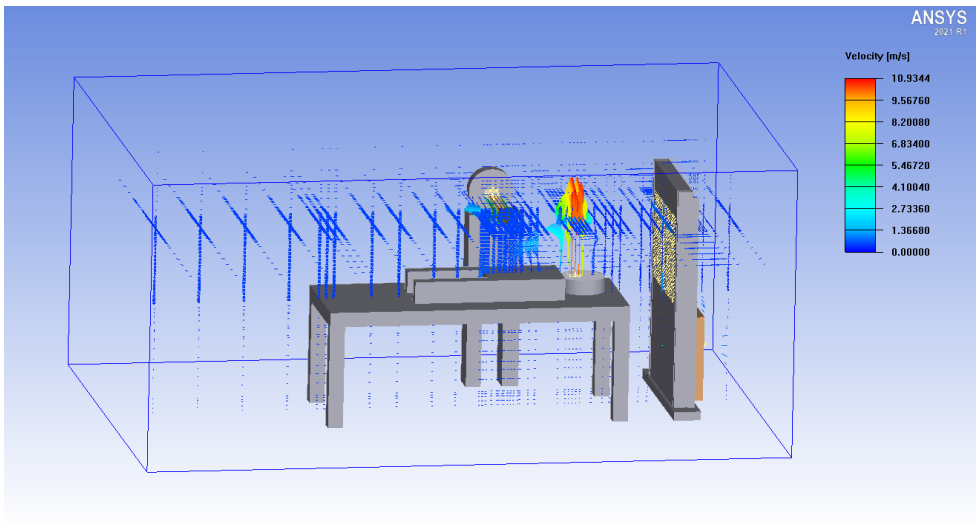

Figure 23. Air purifier top-view simulation in the ward at a low rotation speed −2.

In the same scenario, at a high rotation speed, it is apparent that the airflow from the equipment air outlet is strengthened to form an air wall. This air wall effectively blocks and blows away the air from the human body, as shown in Figure 24. From Figure 24, it can be observed that the formed air wall takes the gas exhaled by the human body into the filter suction end and the airflow, due to the high-pressure circulating filtration.

Case 3: The quarantine station design and the quarantine personnel are well ventilated. The equipment is set to run at low speed. It can be observed from the equipment that the equipment airflow velocity can bring the gas exhaled by the human body into the airflow direction. The air discharged by the human body in the open space can flow out of the space, along with the airflow direction, into the airflow outside the space. After filtering in the inhalation device, filtered air is blown out from the air outlet to the human body position to form a blocking air wall, as shown in Figure 25.

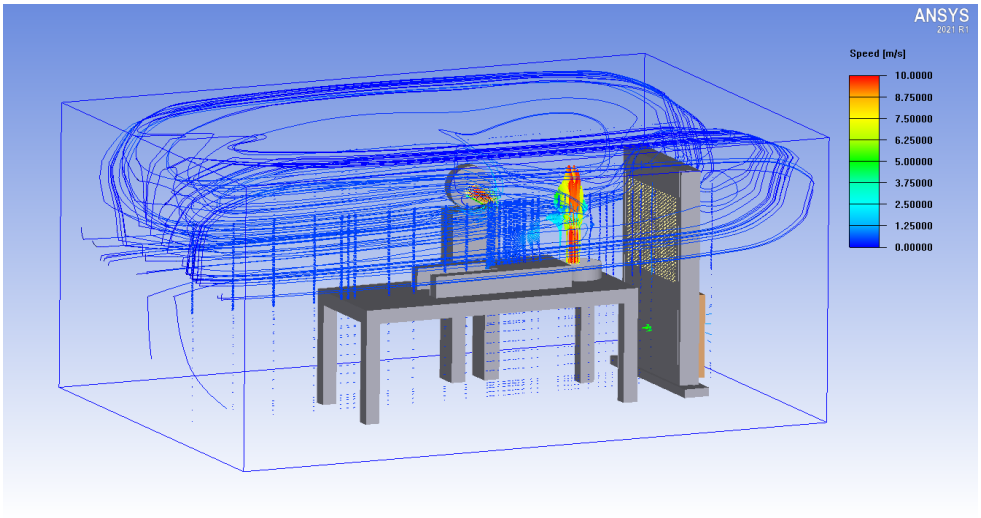

Figure 24. Air purifier simulation in the hospital ward at a high rotation speed.

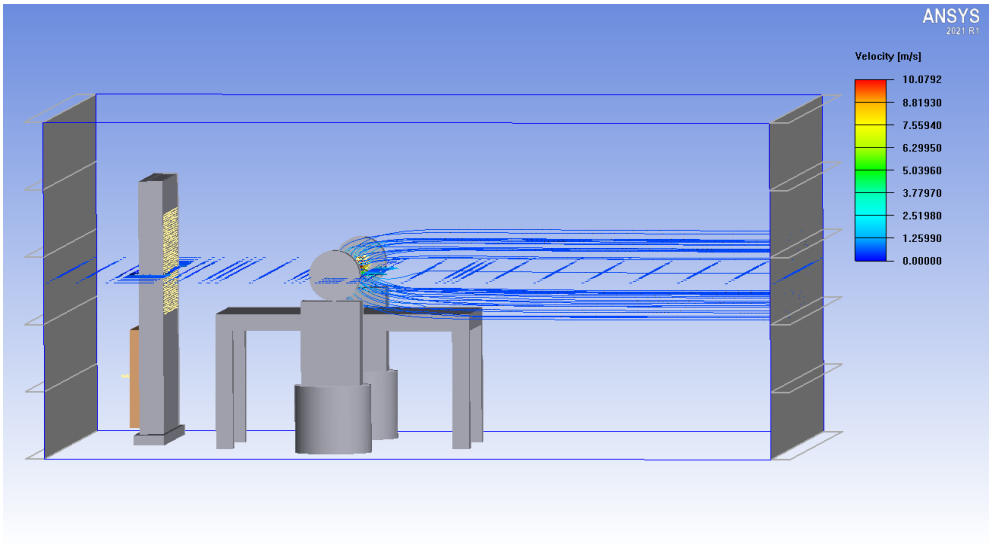

Figure 25. Air purifier simulation in the quarantine station at a low rotation speed.

In the same scenario, at a high rotation speed, it is apparent that the airflow from the equipment air outlet is strengthened to form a gas wall, which effectively blocks and blows away the gas exhaled by the human body, as observed in Figure 26. Due to the high pressure, the gas exhaled by the human body is taken out of the space, so that the gas exhaled by the human body flows out of the semi-open space.

Case 4: This simulation was designed for a conference room with six people sitting at a conference table. The air purifier was set at a low rotation speed. The equipment airflow velocity brings the gas exhaled by the human body into the airflow direction. As shown in the simulation result top view in Figure 27, the gas exhaled by the human body in a confined space follows the airflow direction. Backflow into the equipment's suction end produces a circulation effect, as shown in Figure 28. This allows the indoor air to enter the equipment for circulating filtration.

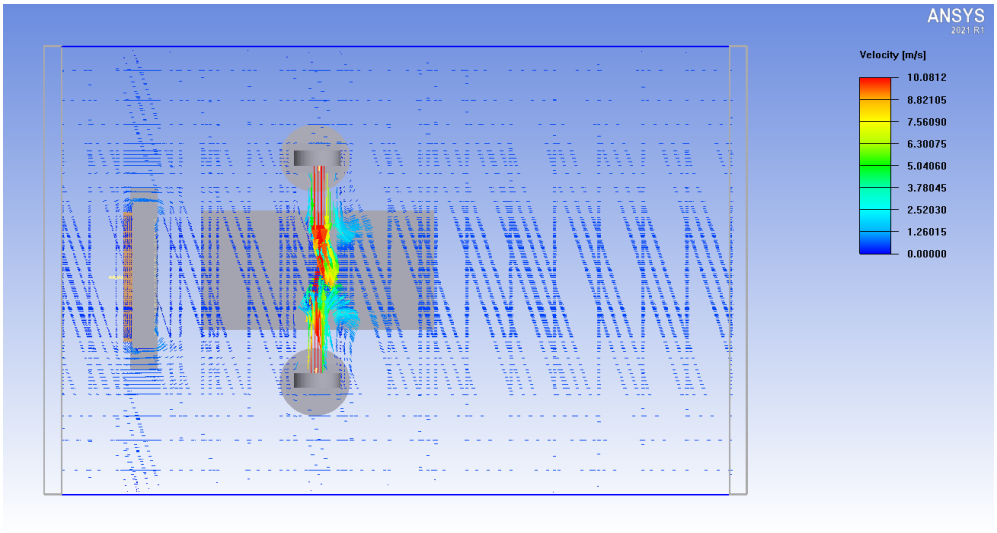

Figure 26. Air purifier top-view simulation in the quarantine station at a high rotation speed.

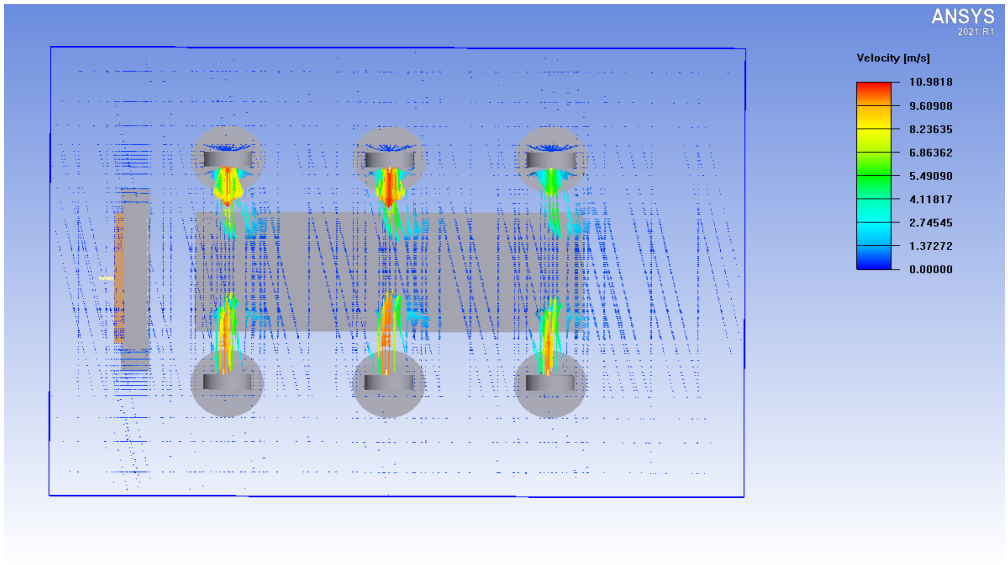

Figure 27. Air purifier simulation top view in the conference room at a low rotation speed −1.

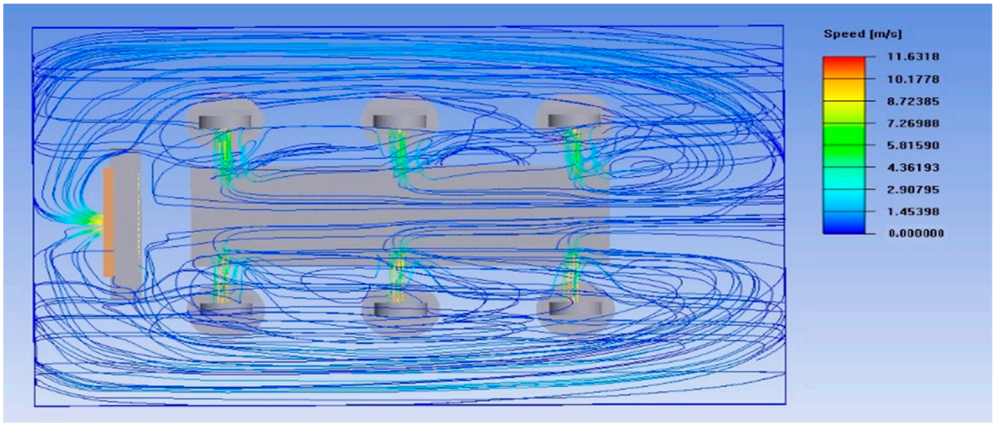

Figure 28. Air purifier simulation top view in the conference room at a low rotation speed −2.

In the same scenario, at a high rotation speed, it is apparent that the airflow from the equipment outlet forms an air curtain, due to the high pressure, blocking the gas discharged from the staff sitting in the conference room, as shown in Figure 29. Based on Figure 30, when people sit in opposite positions, the air purifier sucks the gas exhaled by the human body toward the middle of the conference table, due to the high pressure. A small air wall is formed, which easily affects nearby people. The gas exhaled by the human body can be filtered, so that the air in this space can be regularly purified.

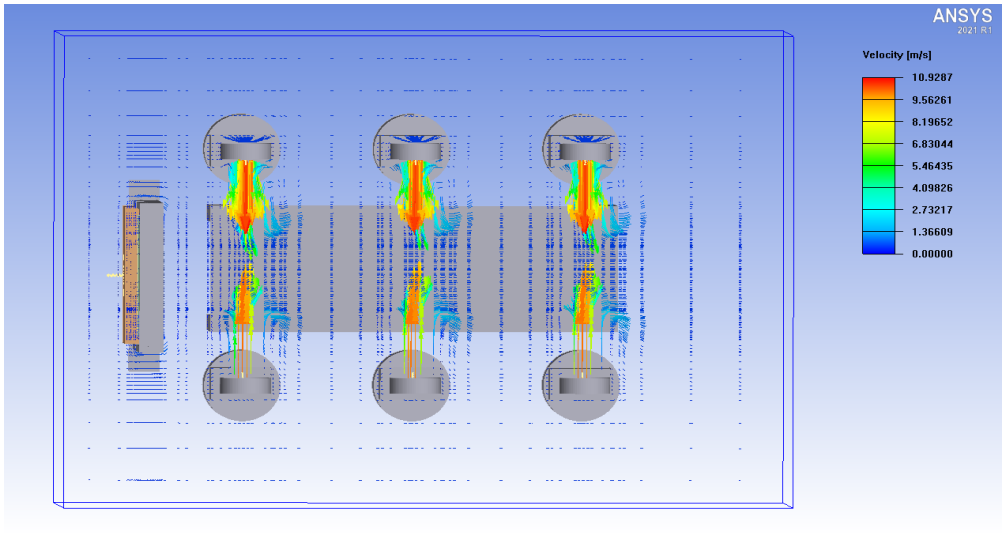

Figure 29. Air purifier simulation top view in the conference room at a high rotation speed −1.

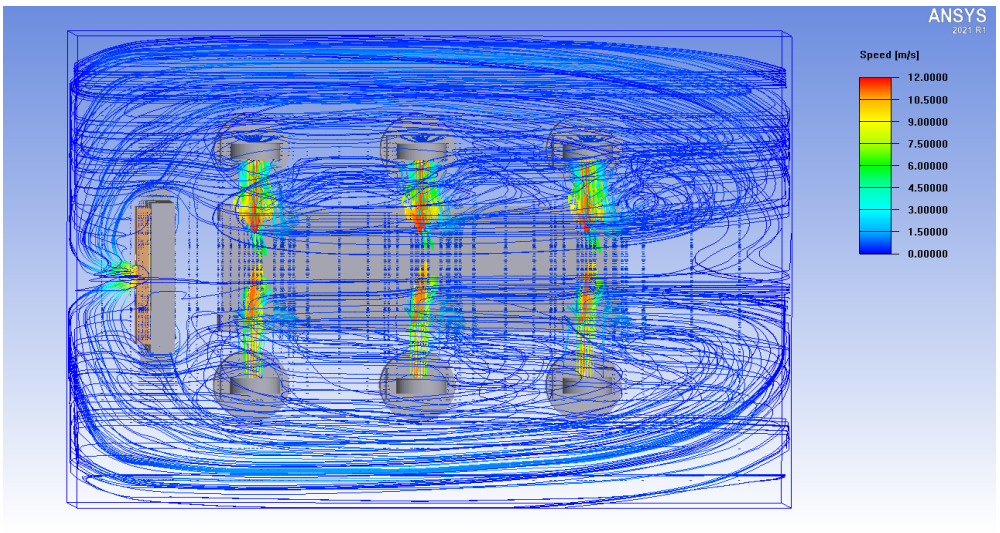

Figure 30. Air purifier simulation top view in the conference room at a high rotation speed −2.

In the same situation, when the rotation speed is high, a circle is built with an opening diameter of 0.06 m for the human body (B, E) sitting in the middle position, as shown in Figure 31. The wind speed (flow specification) is set to ± 1 m/s. The simulation is carried out under the condition that the other settings are not changed. It can be observed from Figure 32 that the gas expelled from the A, D, and B positions will affect the B and E positions. The blocking effect is, therefore, not achieved. This device forms an air wall to block the influence of mutual breath mixing. The partition can be used for protection when sitting next to another person. In the future, ventilation equipment will be added for improvement.

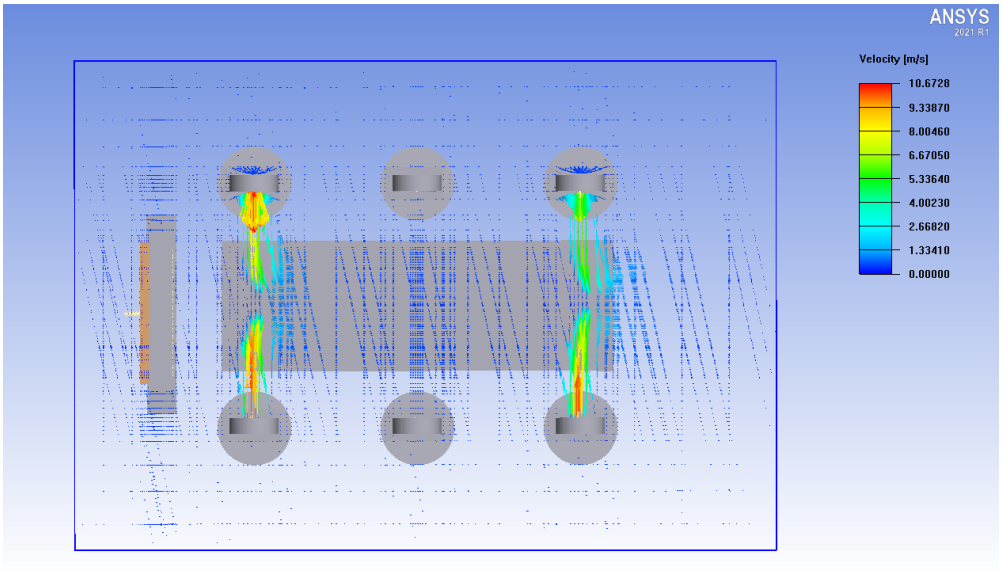

Figure 31. Air purification equipment high-speed simulation results placed in a conference room −1.

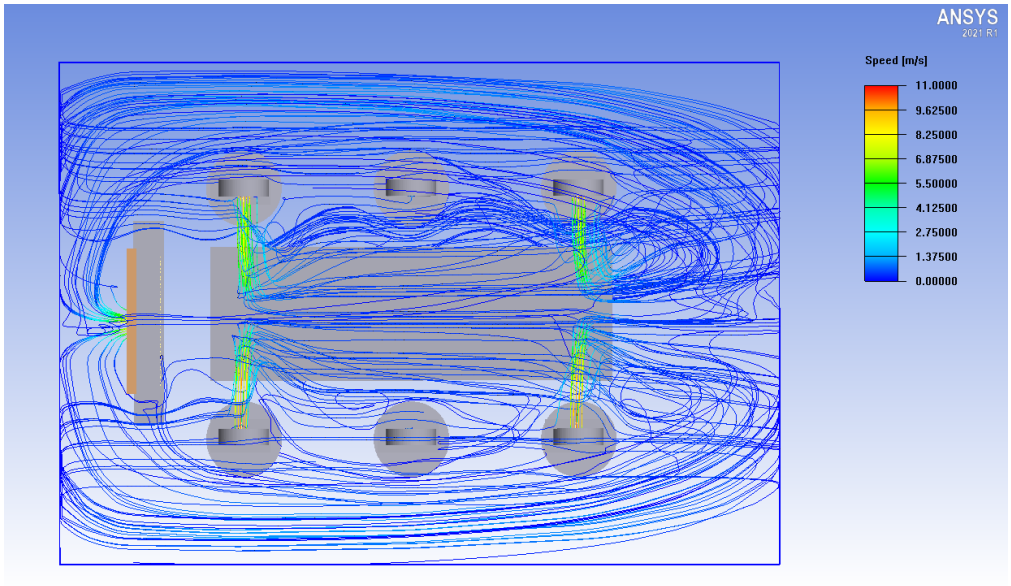

Figure 32. Air purification equipment high-speed simulation results placed in a conference room −2.

According to the simulation, the air purifiers at high and low rotation speeds were compared. The centrifugal fan's velocity and pressure were low at low rotation speeds. The ventilation walls formed at the outlet had barrier effects and were less likely to affect each other, filtering the body's exhaled gas. The centrifugal fan's velocity and pressure were high at high rotation speeds. The ventilation walls formed at the outlet were large. It was easy to inhale the gas discharged from the human body into the air curtain, so that the air flowed from the place with low pressure to the place with high pressure; however, there was no significant barrier effect. According to the simulation, the rotation speed could be adjusted according to different scenarios and the number of people. Consulting rooms and sickbeds could use low rotation speeds, due to the small number of people in those spaces. With effective blocking and screening, quarantine stations can also use low rotation speeds for ventilated spaces. By bringing the gas exhaled by the human body into the meeting room situation, due to the amount of people and the confined space, the gas exhaled by the human body can be quickly brought into the equipment to be filtered at high speed.

4. Conclusions

Whether in an open or closed environment, the simulated air purification equipment of this study can effectively block and purify the harmful substances in the air. In closed or open environmental conditions, the operating speed range of the equipment can be determined according to the number of people. The equipment can be set to run at high speed, increase the air volume, form a wind wall to effectively block the airflow from a person sitting opposite, and reduce the chance of droplet infection. However, note that the rotation speed should not be too high. If the equipment air volume is too large, it easily produces turbulence, deviating the airflow from the intended direction, causing airflow between adjacent people, and increasing the chance of infection. You can choose to increase the distance between adjacent people or add insulation boards between adjacent people to block airflow and reduce the risk of infection.

Author Contributions: Conceptualization, Y.-D.K. and Y.-L.L.; methodology, Y.-D.K. and Y.-L.L.; software, Y.-D.K. and Y.-L.L.; investigation, Y.-D.K. and Y.-L.L.; resources, Y.-D.K.; data curation, Y.-L.L.; writing—original draft preparation, Y.-L.L.; writing—review and editing, Y.-D.K. and W.-J.L.; visualization, Y.-L.L.; supervision, Y.-D.K. and W.-J.L.; project administration, Y.-D.K.; funding acquisition, Y.-D.K. All authors have read and agreed to the published version of the manuscript.

Funding: This research received no external funding.

Institutional Review Board Statement: Not applicable.

Informed Consent Statement: Not applicable.

Data Availability Statement: Data sharing not applicable.

Acknowledgments: The authors acknowledge the equipment provide by New Air Tech throughout this research.

Conflicts of Interest: The authors declare no conflict of interest.

References

1. Chiu, Y.-H.; Tai, Y.-Z.; Wu, M.-F. Using Buoyancy Ventilation Strategy to Improve Indoor Thermal Environment and Ventilation Performance. *Archit. Plan.* **2010**, *11*, 111–135.
2. Gunatilaka, C.C.; Schuh, A.; Higano, N.S.; Woods, J.C.; Bates, A.J. The effect of airway motion and breathing phase during imaging on CFD simulations of respiratory airflow. *Comput. Biol. Med.* **2020**, *127*, 104099. [CrossRef] [PubMed]
3. Cao, Q.; Liu, M.; Li, X. Influencing factors in the simulation of airflow and particle transportation in aircraft cabins by CFD. *Build. Environ.* **2022**, *207*, 108413. [CrossRef]
4. Oh, W.; Ooka, R.; Kikumoto, H.; Han, M. Numerical modeling of cough airflow: Establishment of spatial–temporal experimental dataset and CFD simulation method. *Build. Environ.* **2022**, *207*, 108531. [CrossRef]
5. Sheng, S.; Yamanaka, T.; Kobayashi, T.; Yuan, J.; Katoh, M. Modeling of supply airflow from slot line diffuser on ceiling for CFD of thermal environment in perimeter zone. *Build. Environ.* **2022**, *213*, 108884. [CrossRef]
6. Endar, B.; Nurhandoko, R.K.; Martha, K.T.S.A.; Wibowo, S.W. Airflow Study of a Closed Room in the Public Spaces and Mass Transportation for Healthy and Safe from The Transmission of COVID-19 2020. *J. Perenc. Pembang. Indones. J. Dev. Plan.* **2021**, *5*, 20–31.
7. Yang, A.; Holøs, S.B.; Resvoll, M.O.; Mysen, M.; Fjellheim, Ø. Temperature-Dependent Ventilation Rates Might Improve Perceived Air Quality in a Demand-Controlled Ventilation Strategy. *Build. Environ.* **2021**, *205*, 108180. [CrossRef]
8. Sui, X.M.; Tian, Z.J.; Liu, H.T.; Chen, H.; Wang, D. Field Measurements on Indoor Air Quality of a Residential Building in Xi'an under Different Ventilation Modes in Winter. *J. Build. Eng.* **2021**, *42*, 103040. [CrossRef]
9. Xu, J.C.; Guo, H.; Zhang, Y.L.; Lyu, X.P. Effectiveness of personalized air curtain in reducing exposure to airborne cough droplets. *Build. Environ.* **2021**, *208*, 108586. [CrossRef]
10. Wang, Y.-H. Design and Analysis of Ambient Heat Flowin Quartz GlassTubing Processing Room Field. Master's Thesis, National Chin-Yi University of Technology, Taichung City, Taiwan, 2019.
11. Lu, C.-Y. Study on Control Efficiency and Cost of Fine Suspended Particles by Filters Used in Commercial Air Purifiers. Master's Thesis, Jinwen University of Science and Technology, New Taipei City, Taiwan, 2019.
12. Thi Dao, H.T.; Kim, K.-S. Behavior of cough droplets emitted from Covid-19 patient in hospital isolation room with different ventilation configurations. *Build. Environ.* **2022**, *209*, 108649.
13. Benchrif, A.; Wheida, A.; Tahri, M.; Ramiz, M.; Biswas, S. Air Quality during Three COVID-19 Lockdown Phases: AQI, PM2.5 and NO_2 Assessment in Cities with More than 1 Million Inhabitants. *Sustain. Cities Soc.* **2021**, *47*, 103170. [CrossRef] [PubMed]

14. Agarwal, N.; Meena, C.S.; Raj, B.P.; Saini, L.; Kumar, A.; Gopalakrishnan, N.; Kumar, A.; Balam, N.B.; Alam, T.; Kapoor, N.R.; et al. Indoor Air Quality Improvement in COVID-19 Pandemic: Review. *Sustain. Cities Soc.* **2021**, *70*, 102942. [CrossRef]
15. Sahraei, M.A.; Kuşkapan, E.; Çodur, M.Y. Public Transit Usage and Air Quality Index during the COVID-19 Lockdown. *J. Environ. Manag.* **2021**, *286*, 112166. [CrossRef] [PubMed]
16. Jahanbin, A. Efficacy of Coupling Heat Recovery Ventilation and Fan Coil Systems in Improving the Indoor Air Quality and Thermal Comfort Condition. *Energy Built Environ.* **2021**. [CrossRef]
17. Zhu, Y.-D.; Li, X.; Fan, L.; Li, L.; Wang, J.; Yang, W.-J.; Yao, X.-Y.; Wang, X.-L. Indoor Air Quality in the Primary School of China—Results from CIEHS 2018 Study. *Environ. Pollut.* **2021**, *291*, 118094. [CrossRef] [PubMed]
18. Raheja, S.; Obaidat, M.S.; Sadoun, B.; Malik, S.; Rani, A.; Kumar, M.; Stephan, T. Modeling and Simulation of Urban Air Quality with a 2-Phase Assessment Technique. *Simul. Model. Pract. Theory* **2021**, *109*, 102281. [CrossRef]
19. Da Conceição Pereira, P.F.; Broday, E.E.; de Paula Xavier, A.A. Thermal Comfort Applied in Hospital Environments: A Literature Review. *Appl. Sci.* **2020**, *10*, 7030. [CrossRef]
20. Sung, W.-P.; Chen, T.-Y.; Liu, C.-H. Strategy for Improving the Indoor Environment of Office Spaces in Subtropical Cities. *Buildings* **2022**, *12*, 412. [CrossRef]
21. Pease, L.F.; Wang, N. A missing layer in COVID-19 studies: Transmission of enveloped viruses in mucus-rich droplets. *Int. Commun. Heat Mass Transf.* **2022**, *131*, 105746. [CrossRef]
22. Mixture Model Theory. *ANSYS Fluent Theory Guide*; Ansys, Inc.: Canonsburg, PA, USA, 2020; Volume R1, pp. 593–603.
23. Ansys, Inc. *Ansys Icepak User's Guide*; Ansys, Inc.: Canonsburg, PA, USA, 2021; Volume R2, pp. 257–269.
24. MayAir, D-Guard5. Available online: http://www.mayair.com.tw/items/8e3f1e (accessed on 20 March 2022).